Validation and Calibration of Conceptual Design Tool SUAVE

Conor Gallagher[1], Charles Stuart[2], Stephen Spence[3]
Trinity College Dublin, the University of Dublin, Ireland

Thomas Fowler[4]
Ryanair

The aim of this study is to provide a comprehensive validation of the conceptual design tool SUAVE, with respect to real world flight data from an extensive flight database of 737-800NG fleet operations. A validation of the initial SUAVE model fuel burn predictions was performed and compared with the actual data. A surrogate propulsion model was developed using NPSS and integrated into SUAVE, which significantly enhanced the model accuracy. A calibration of the SUAVE aerodynamic model coefficients, the propulsion model idle throttle value, and the take-off and landing drag increments was performed which aimed to minimise the fleet-wide fuel burn error with respect to the actual flight data within the database. The model was calibrated using 26 case flights in a training database, and the final calibrated model performance was measured against three unseen test cases within the flight database. A modest reduction in error was observed for the training and test cases, however non-linear error effects in the presence of headwinds and tailwinds affected the model accuracy and limited the potential of the calibration. Despite these effects, a highly accurate model was developed with an average fuel-flow error of 5% with respect to real-world flight data, providing an accurate baseline model from which confident projections of future carbon reductions can be obtained for new aircraft designs.

I. Nomenclature

ADS-B	=	Automatic Dependent Surveillance-Broadcast
EDS	=	Environmental Design Space
FLOPS	=	Flight Optimisation System
GS	=	Ground Speed
NM	=	Nautical Miles
NPSS	=	Numerical Propulsion System Software
e-SAF	=	Synthetic Sustainable Aviation Fuel
SAF	=	Sustainable Aviation Fuel
SLS	=	Sea-Level Static
SUAVE	=	Stanford University Aerospace Vehicle Environment
TAS	=	True Airspeed
TASOPT	=	Transport Aircraft System Optimisation
TSFC	=	Thrust Specific Fuel Consumption
UHAR	=	Ultra-High Aspect Ratio
VLM	=	Vortex-Lattice Method
C	=	Correction factor
C_D	=	Drag coefficient
$C_{D,p}$	=	Fuselage parasite drag coefficient
C_f	=	Skin friction coefficient
k	=	Form factor
Ma	=	Mach number
S_{ref}	=	Reference area
V	=	Velocity
α	=	Wind correction factor
δ	=	True course
ω	=	Wind direction

[1] Ph.D. Student, Department of Mechanical, Manufacturing and Biomedical Engineering.
[2] Assistant Professor, Department of Mechanical, Manufacturing and Biomedical Engineering.
[3] Professor, Department of Mechanical, Manufacturing and Biomedical Engineering.
[4] Director of Sustainability & Finance

II. Introduction

A. Context and Motivation

This study considers the calibration and validation of an aircraft modelling tool against a broad spectrum of real flight data from a large aircraft fleet as a method to evaluate decarbonisation steps for aviation. Pathways to net-zero have been suggested in a bid to reach the ambitious targets set by the industry for 2050. Sustainable Aviation Fuel (SAF) is envisaged to be the main driver of decarbonisation [1], however, bio-derived feedstocks are limited and compete with food and general land use, and are therefore not considered sustainable in the long term [2]–[4], whereas synthetic SAF (e-SAF) requires a considerable amount of renewable electricity for its production. Synkero, a start-up company for the production of e-SAF, claim that 30 off-shore wind turbines (1,200 GWh) would be required for the production of 1% of all fuel used at Amsterdam Schiphol airport during 2019 [5]. Furthermore, if all 95 billion gallons of jet fuel consumed by commercial airlines globally in 2019 were to be replaced with e-SAF, it could demand between 244-489% of all wind and solar electricity generated in 2021, based on e-SAF production efficiencies of 25-50% [6], [7]. The significant scale of the renewable electricity required affects the availability and cost of e-SAF. Therefore, efficiency improvements for aircraft are of paramount importance in reducing the overall energy demand of aviation, and hence the demand for expensive sustainable fuels for decarbonisation.

Research and development of several novel concepts for next-generation aircraft is ongoing, including evolutionary concepts such as ultra-high bypass ratio turbofans and Ultra-High Aspect Ratio wings (UHAR), whereas more disruptive technologies include open-rotor engines, hybrid-electric propulsion systems or the blended-wing body. Such concepts require effective conceptual design tools for rapid, low-fidelity simulations with sufficient accuracy. Furthermore, such unconventional designs require physics-based models to investigate new design envelopes, outside the boundaries where traditional empirical correlations are no longer valid.

B. Evaluation of Conceptual Design Tools

Many conceptual design tools have been developed in recent years, such as Flight Optimisation System (FLOPS) [8], Transport Aircraft System Optimisation (TASOPT) [9], Environmental Design Space (EDS) [10], and Stanford University Aerospace Vehicle Environment (SUAVE) [11]. Table 1 provides details of popular conceptual design tools used in recent published literature.

Table 1 Description of popular conceptual design tools in published literature

Design Tool	Modelling Techniques	Unconventional Aircraft Capabilities	Design Flexibility	Availability
FLOPS	Empirical weight correlations with physics-based mission analysis	Only possible with workarounds and manipulation of the tool coupled with external software	Can be coupled with some external software, code makes key assumptions that limits flexibility (e.g. fuel must be consumed)	Broad availability, not open-source
TASOPT	Low-order physics-based models – empirical correlations where necessary	Strong for boundary-layer ingestion, issues with electric aircraft due to lack of mission flexibility	Always optimises vehicles for specific mission – issues with pre-sized aircraft. Requires detailed input information	Broad availability, not open-source
EDS	Physics-based or surrogate models, empirical for conventional designs	Unconventional designs have been modelled, limitations unclear	Requires coupling with several external NASA design tools	FAA tool. Unavailable to general public
SUAVE	Physics-based and semi-empirical models – depending on fidelity & analysis required	Unconventional aircraft easily modelled for experienced users	Multi-fidelity framework – couple with external tools OpenVSP, SU2, OpenMDAO, import propulsion / aerodynamic surrogates	Broad availability and open-source with simple recompiling

SUAVE was selected as the conceptual design tool for this analysis, due to its broad availability, open-source framework to allow for development and customisation, multi-fidelity approach and physics-based models. Some of

these physics-based methods, such as the aerodynamic Vortex-Lattice Method (VLM) and Blade Element Momentum Theory (BEMT), were recently validated against wind tunnel data [12], [13]. VLM is a low-fidelity aerodynamic calculation method, which discretises the wing into panels and makes use of the Biot-Savart law to calculate the inviscid lift [14]. An important aspect of the SUAVE's low-fidelity VLM module is the capability for calibration through semi-empirical methods, since the calculation uses a number of correction factors to complete the lift and drag calculations.

C. Objectives

SUAVE has gained popularity as a tool for aircraft design and analysis in recent published literature [15]–[19], however it lacks a thorough, comprehensive validation against complete, current aircraft designs. For example, the SUAVE developers validated a Boeing 737-800 aircraft model by comparing the block fuel burn of the design mission with that of similar design tools [11], while a recent study of a UHAR aircraft validated the SUAVE fuel burn results against a similar Boeing numerical study [16]. This study aims to progress the validation of SUAVE further, by comparing model results with real-world flight data. Specific objectives of this work include:

- Development of the SUAVE model for the Boeing 737-800NG aircraft
- Development and validation of the NPSS propulsion model for the CFM56-7B26/3 turbofan
- Model at least 25 real-world flights with significant variation in payload and range
- Validate the predicted average fuel-flow of each flight segment against actual fuel burn data
- Explore the potential for calibration through optimisation of correction factors applied to VLM
- Compare the optimised calibrated model performance against the baseline model performance

The aim of this study is to provide a detailed validation of the SUAVE simulation framework, by comparing the model's fuel burn results with real-world flight data, for a variety mission payloads and ranges. The flight data for this study has been provided by Ryanair – Ryanair is Europe's leading passenger airline, operating a fleet of 471 Boeing 737 aircraft, with up to 3000 flights daily [20]. The company's extensive database of flight data with details of fuel burn and take-off weights provided a valuable opportunity for broader validation and calibration of the SUAVE aircraft modelling tool, the results of which can increase the confidence in its use in other research studies to decarbonise future aircraft.

III. Methodology

A. Real-World Operations

1. Flight Database

The flight database contained flight data from an airline, such as take-off weights and average fuel-flow per flight segment, for 29 flights for Boeing 737-800NG aircraft over a two day period. The distribution of the sample flights is presented in Fig. 1 in terms of flight range and Take-off Weight (TOW), where TOW values have been redacted due to the sensitive nature of the data. Three test cases with varying flight range were selected to assess the performance of the model calibration, which is detailed in Section V.

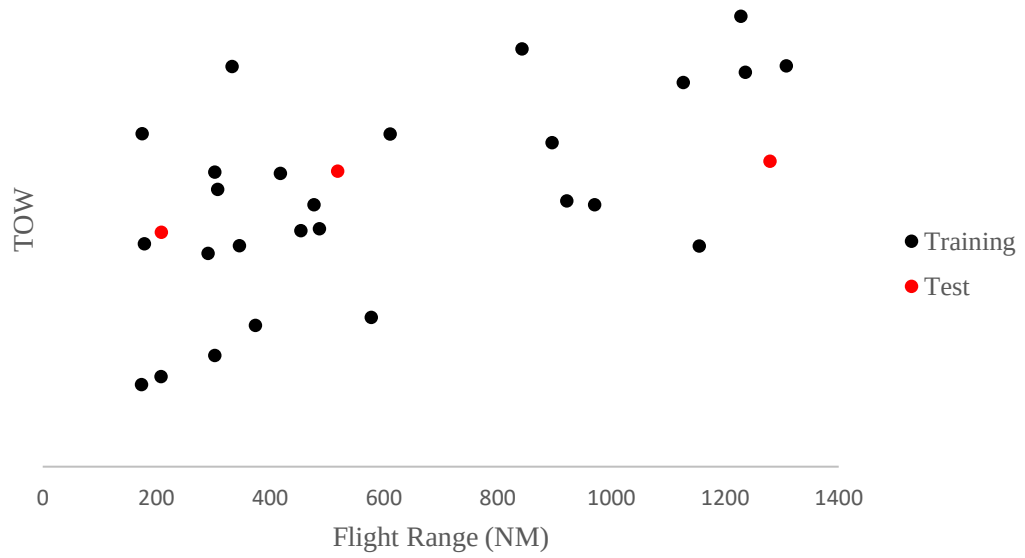

Fig. 1 Distribution of B737-800NG missions from available flight database in terms of range and TOW

2. Flight Paths

Real flight paths were obtained from Automatic Dependent Surveillance-Broadcast (ADS-B) data to ensure the validation models were representative of real-world conditions. Publicly available timestamped coordinates were downloaded, from which the flight path in terms of altitude and speed was calculated using a MATLAB software routine. The flight path was approximated using linear piece-wise segments, outlining information such as the initial and terminal altitude, initial and terminal speed, and the rate of climb/descent to be input to SUAVE for each segment.

The climb and descent segments each consisted of 18 linear sub-segments to ensure an accurate representation of the flight paths. Cruise was approximated using a single, level, linear segment with a constant speed and constant altitude, ignoring any step-climb/descent operations. The initial climb, approach, and final approach segments, which are separated from climb and descent due to the deployment of flaps and landing gear, were each represented by a single sub-segment using the same parameters as climb and descent.

It is important to note that the True Airspeed (TAS) profile was unavailable for these flights, hence the effect of wind speed is unaccounted for in the current analysis. Instead, the model calculates the speed of the aircraft as seen from a stationary observer, i.e. the Ground Speed (GS). Hence, the TAS was equal to the ADS-B derived GS, and this model is referred to as the GS model for the remainder of the paper. The significance of omitting wind speed is analysed and discussed in Section IV.C. An example of the flight path approximation for a mission from the flight database is presented in Fig. 2.

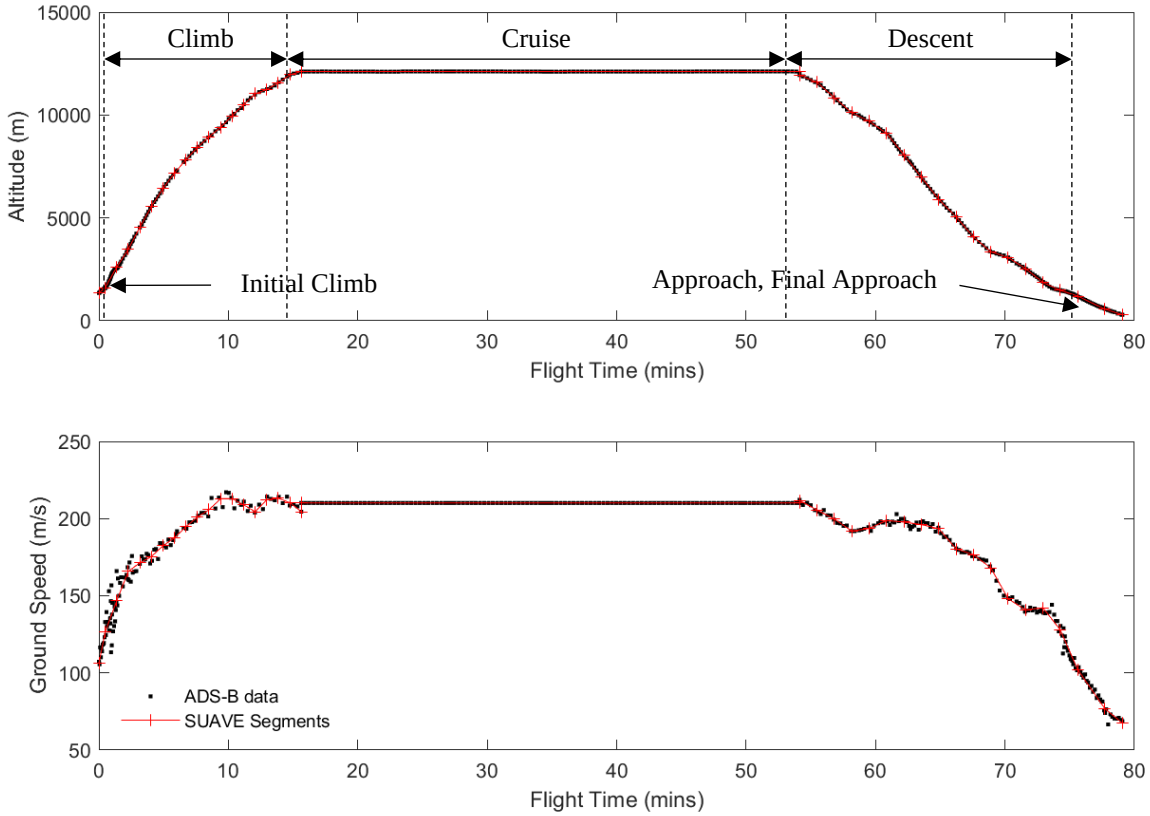

Fig. 2 Flight path altitude and speed approximation for SUAVE input

B. Aircraft Model

1. Boeing 737-800NG

A Boeing 737-800NG model was developed using SUAVE, using detailed airframe geometry information obtained from [21]. The initial propulsion system design was based on the CFM56-7B26 turbofan, with information obtained from [22]. The built-in propulsion model within SUAVE uses a simplified analysis based on the methods of Cantwell [23], and approximates the performance by using a single operating point efficiency, based on the design point efficiency. As a result, the SUAVE propulsion model does not account for off-design efficiency, and thus the Thrust Specific Fuel Consumption (TSFC) is a function of only the altitude and Mach number. An example of the simplistic propulsion modelling in SUAVE can be seen in the work of Dorsey and Uranga [19], which used fixed stage efficiencies and pressure ratios throughout the propulsion system simulations.

2. Aerodynamics

The aerodynamic model used within SUAVE is known as the 'Fidelity-Zero' model, which is based on the Vortex-Lattice Method (VLM). The VLM is used to calculate the inviscid lift through discretisation of the wing into panels, and calculation of the strength of the trailing vortices and their downwash effect using the Biot-Savart law using an assumed circulation distribution [14]. Factor based corrections to account for the lift effects of the fuselage, compressibility, and viscous effects are applied to the inviscid wing lift to obtain the total aircraft lift [11].

The aircraft drag is comprised of the parasite drag, lift-induced drag, compressibility drag and miscellaneous drag. The parasite drag is the drag associated with skin friction and pressure drag, and is computed for the fuselage, wings and nacelles. The fuselage and wing parasite drag is calculated using Eq. (1), where C_f is the skin friction coefficient, S_{ref} is the reference area, and k is the form factor which varies for each calculation [11]. The lift-induced drag is composed of viscid and inviscid components. The inviscid lift-induced drag is obtained from the VLM calculation, while the viscid component is calculated using a viscous lift-dependent drag factor [11]. The compressibility and

miscellaneous drag is calculated using correlations from Shevell [24] and Kroo [25]. More information on this aerodynamic model can be obtained from [11].

$$C_{D_P} = k \cdot C_f \cdot S_{ref} \tag{1}$$

3. Mission Solver

The SUAVE mission solver works by iterating the unknowns of a mission segment, generally the throttle and pitch angle, until the residuals are converged. In the case of cruise, the residuals are the sum of horizontal and vertical forces, which are converged to zero [11]. For the climb and descent segments, a 'linear speed, constant rate' segment was used, which models an accelerating/decelerating aircraft moving with a constant vertical rate of climb/descent. The cruise segment was modelled using a 'constant speed, constant rate, loiter' segment, which models an aircraft with steady, constant altitude motion for a prescribed length of time.

C. Propulsion Model

1. CFM56-7B26/3

The simplistic nature of the SUAVE propulsion model was noted in the previous section. However, SUAVE was designed to be used as a flexible design tool with multi-fidelity capabilities, allowing simple integration of external design tools to increase the fidelity of the analysis where necessary. This is an important strength of the SUAVE modelling tool. To analyse the influence of the propulsion system inaccuracies within the current study, NASA's Numerical Propulsion System Software (NPSS) [26] was used to develop a surrogate propulsion model of the CFM56-7B26 engine to be integrated within the overall SUAVE aircraft model, enabling accurate off-design propulsion analysis through the use of component performance maps. The surrogate model was generated using Gaussian process regression methods, which formulates a continuous function for thrust and TSFC based on the nearby points of the discrete NPSS dataset, using a normal distribution [27]. NPSS was chosen as the propulsion system software due to the extensive use of the tool throughout published literature for both existing and unconventional designs [28]–[32], along with the presence of documented validations [32]–[34], combined with the collective experience of contributors NASA and consortium members such as GE Aviation, Boeing, Rolls-Royce, Lockheed Martin and others [35].

Fig. 3 illustrates the CFM56 turbofan model in block diagram form, outlining the various components used within the model. The model was calibrated to match International Civil Aviation Organisation (ICAO) testbed data for Sea-Level-Static (SLS) operating points, in which the component design variables were used to vary the model outputs. Component design variables include compressor/turbine pressure ratios and stage efficiencies, along with the combustor outlet temperature and the bypass ratio. For off-design analysis, generalised component performance maps were used, based on a late 1980's advanced technology turbofan developed by NASA in their energy efficient engine programme [36].

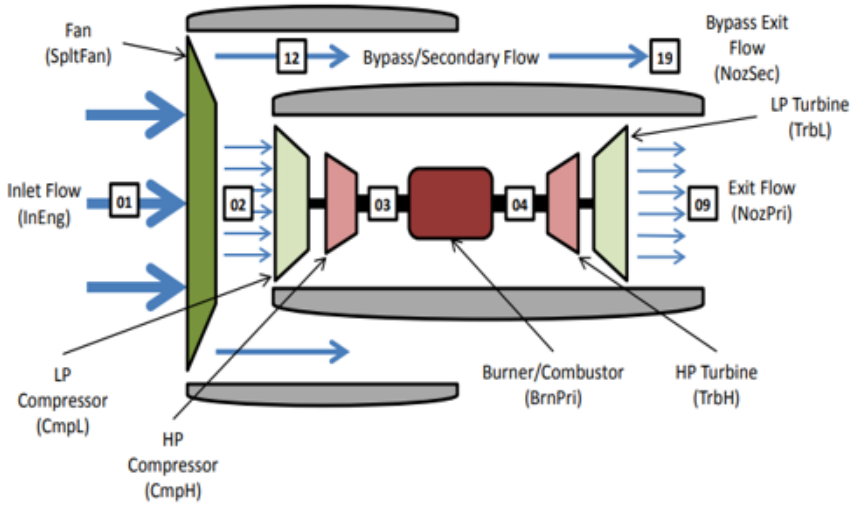

Fig. 3 Block diagram of NPSS CFM56-7B26/3 turbofan model [35]

2. Validation

The final validation results of the calibrated turbofan model are presented in Table 2. Validation errors are calculated with respect to the ICAO SLS data, obtained from the ICAO Emissions Databank [37], along with published CFM56-7B TSFC values for top-of-climb and rolling take-off operating points from a NASA numerical study [34]. The exact engine variant modelled by NASA in that publication is unclear, hence there is uncertainty in these reported TSFC figures. The propulsion model had a high level of accuracy, with the TSFC for three out of four SLS points predicted within 1% accuracy of the measured values. The largest TSFC error occurred for the 30% power point at SLS, with a relative error of -5.71%. This outlier in the validation results may be explained by the use of the generalised component performance maps, since the shape of the speedlines could vary significantly with respect to the actual, proprietary performance maps of the CFM56 turbofan. While this error is relatively insignificant due to the low fuel-flow values at this operating point, further improvements could be obtained through using an optimiser to calibrate the component design variables, and generate scaling coefficients for the component performance maps in order to minimise the validation errors.

Table 2 NPSS validation results for CFM56-7B26/3 turbofan model

Operating Point	Thrust (lbf)	Thermal Eff.	Predicted TSFC (lbm/hr.lbf)	NASA/ICAO TSFC	Error
Top-of-Climb	5960	54%	0.635	0.650	-2.31%
Rolling-Take-Off	20954	46%	0.473	0.474	-0.21%
SLS – 100% power	26300	46%	0.369	0.366	0.82%
SLS – 85% power	22355	45%	0.352	0.350	0.57%
SLS – 30% power	7890	32%	0.314	0.333	-5.71%
SLS – 7% power	1841	15%	0.464	0.466	-0.43%

IV. Validation Results

A. SUAVE Validation

An initial validation of SUAVE was performed by comparing the predicted fuel-flow of the initial, unchanged SUAVE model for a sample mission against the actual fuel-flow data within the flight database. The sample mission was a flight of approximately 1300 NM, and the initial SUAVE model used the built-in SUAVE propulsion model (Cantwell [23]) along with the initial 'Fidelity-Zero' VLM aerodynamic model. Fig. 4 shows the predicted fuel-flow and corresponding fuel burn for this model, while Fig. 5 presents the validation of these predictions against the actual flight data. The presented fuel-flow and fuel burn data throughout this study have been non-dimensionalised due to the sensitive nature of the data.

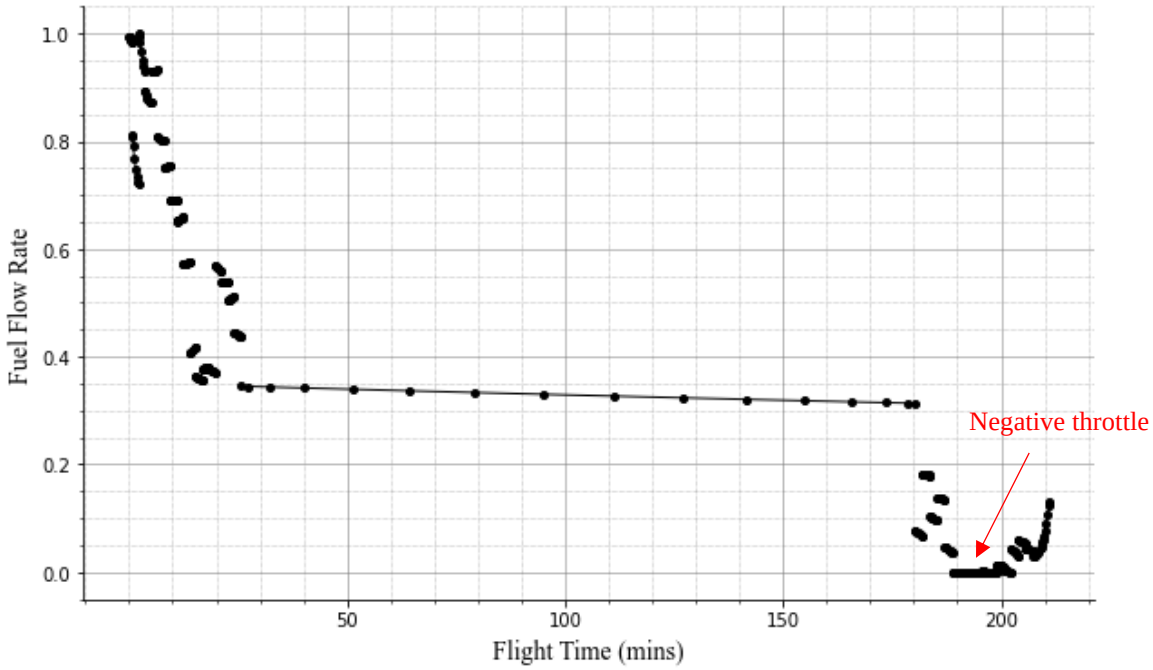

Fig. 4 Initial SUAVE model predictions of B737-800NG fuel-flow for a 1300 NM mission

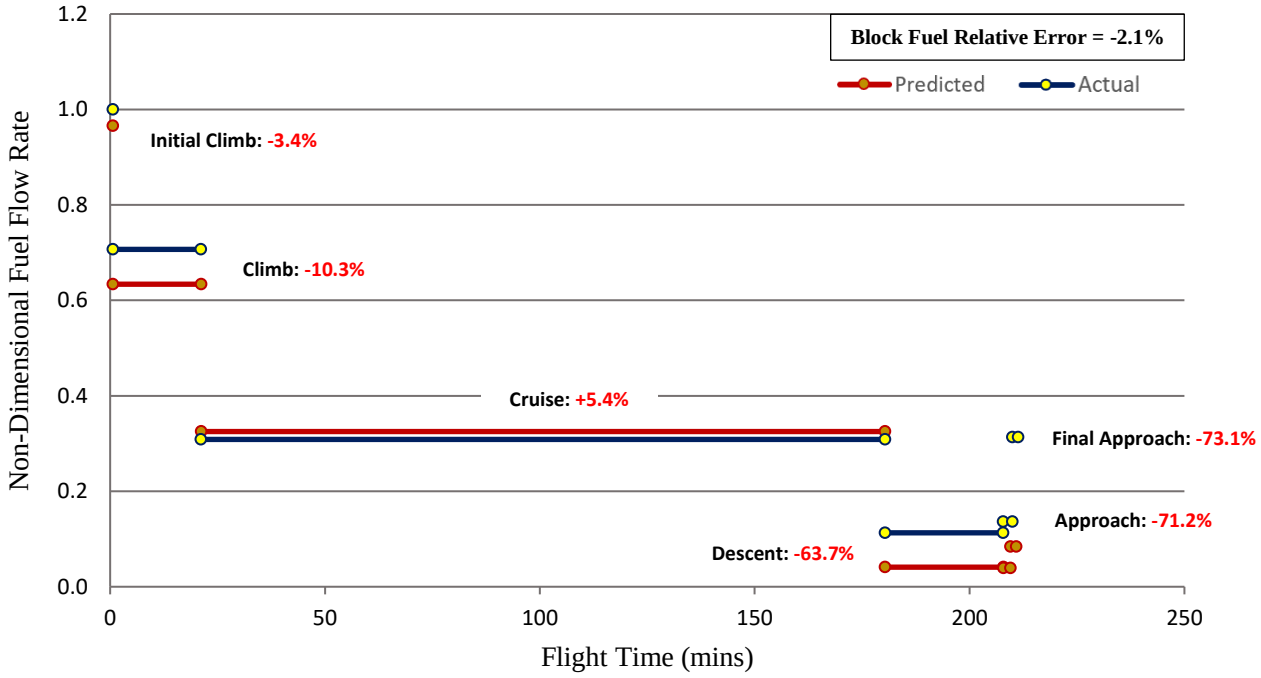

Fig. 5 Validation of Initial SUAVE B737-800NG model against actual flight data (1300 NM)

The model performed reasonably well for the climb and cruise segments. The initial climb and climb fuel-flow was under-predicted with a relative error of 3.4% and 10.3%, respectively, while the cruise segment fuel-flow was over-predicted with a relative error of 5.4%. The accuracy dropped significantly for the descent and approach phases, with under-predictions between 63.7% and 73.1%. The drop in accuracy during these phases was primarily due to several zero fuel-flow segments, associated with the negative throttle segments highlighted in Fig. 4. These zero fuel-flow segments were caused by the solver demanding negative throttle, as the aircraft demanded a higher drag to satisfy

the deceleration requirements imposed by the flight path approximation outlined in Section III.A.2. Of course, in reality the aircraft would still consume some fuel as the engine is throttled back to an idle state, hence these zero fuel-flow segments were unrealistic. Despite the large inaccuracies in the descent phases, the total block fuel consumption was under-predicted by just 2.1%, as the over-prediction of the cruise segment was essentially balanced by the under-predictions of the remaining segments. This emphasises the importance of performing detailed validations where possible, analysing the fuel-flow accuracy per segment rather than the total mission fuel burn, in which the latter is common practice in published research [16].

B. SUAVE-NPSS Validation

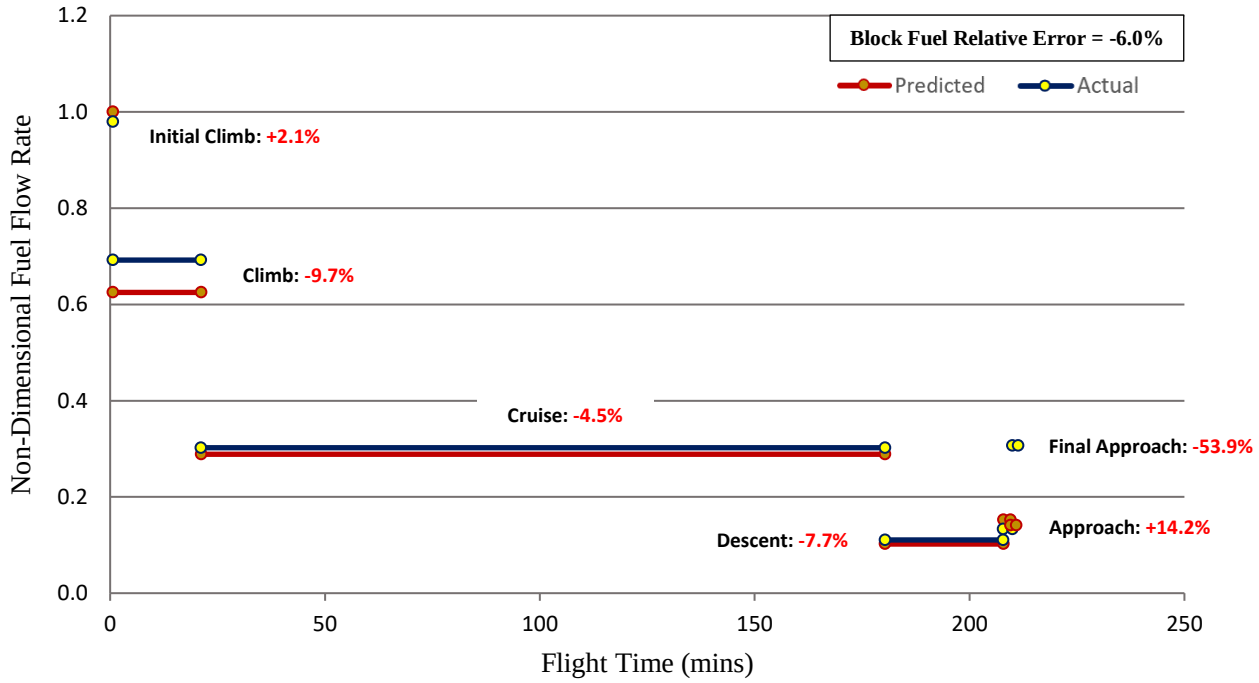

Fig. 6 Validation of SUAVE-NPSS B737-800NG model against actual flight data (1300 NM)

Fig. 6 shows the validation of the SUAVE-NPSS model against the actual flight data for the same flight presented in the previous section. Inclusion of the NPSS propulsion had a substantial effect on fuel-flow performance – the fuel-flow of the cruise segment was reduced to yield an under-prediction of 4.5%, while the descent and approach phase errors improved significantly. The under-prediction of descent improved from a relative error of -63.7% to -7.7%. This was primarily due to the minimum idle fuel-flow applied to the propulsor surrogate, in which segments with negative throttle were set to an idle power setting of 7%. The approach segment yielded a similar improvement, whereas the final-approach segment showed some improvement, but a large under-prediction of 53.9% remained. The initial climb and climb segments showed minor improvements – initial climb was over-predicted by 2.1%, whereas climb was under-predicted by 9.7%. Despite the reduction in relative error for all segments, the block fuel relative error magnitude increased to an under-prediction of 6%. Again, this highlights the issues with validating design tools against total fuel burn performance, as it fails to capture the accuracy of the model against actual performance in different flight segments. Table 3 compares the total fuel burn and average total fuel-flow errors for the 26 flights for the initial SUAVE and the SUAVE-NPSS models. When considered across the collection of different flights, the combined SUAVE-NPSS model almost halved the fuel burn error without any recalibration for specific flights, and displayed significantly superior performance due to the more comprehensive propulsion model.

Table 3 Total fuel burn and fuel-flow errors for the SUAVE and SUAVE-NPSS model

Model	Total Fuel Burn Error	Average Total Fuel-Flow Error
SUAVE	13.4%	9.41%
SUAVE-NPSS	7.5%	5.53%

C. Effect of Wind Speed

The TAS for the missions within the flight database was unavailable for the current analysis. To analyse the effect of wind speed on flight performance, an estimated average wind speed was applied to the two longest flights (outward and return) within the database, which had a range of approximately 1300 NM. The average wind speed was estimated by interactively tracking each flight from an online ADS-B tool. It was found that for the outward route, an average headwind of approximately 18 m/s was present, while for the return route an average tailwind of approximately 20 m/s was present. The SUAVE code was developed to account for wind speed in the analysis, and the flights were re-modelled with a constant 20 m/s headwind/tailwind, and compared to the initial GS model. Eq. (2) shows the calculation used to incorporate the wind speed in to SUAVE, where V is velocity, δ is the true course of the aircraft, ω is the wind direction, and α is the wind correction angle, as defined in Eq. (3).

$$V_{ground} = \sqrt{V_{true}^2 + V_{wind}^2 - 2(V_{true} \cdot V_{wind} \cdot \cos(\delta - \omega + \alpha))} \tag{2}$$

$$\alpha = \sin^{-1}\left(\frac{V_{wind}}{V_{true}} \cdot \sin(\omega - \delta)\right) \tag{3}$$

1. Headwind

With the 20 m/s headwind applied, the TAS became equal to 220 m/s, while the GS was equal to 200 m/s. This was in contrast to the GS model used in this study, in which TAS = GS = 200 m/s. As fuel-flow performance was related to the aircraft TAS, it was clear that the GS model would under-predict the fuel consumption for a mission that experiences a headwind. The results for the outward route with a 20 m/s headwind are presented in Fig. 7, where the GS model produced an average normalised fuel-flow of 28.2% during the cruise segment, while the wind-modified model that accounted for TAS predicted an increased fuel-flow rate of 30.2%. The wind model for the headwind flight produced a cruise fuel-flow error of -2.2% with respect to the actual flight data, compared to -4.5% with the GS model.

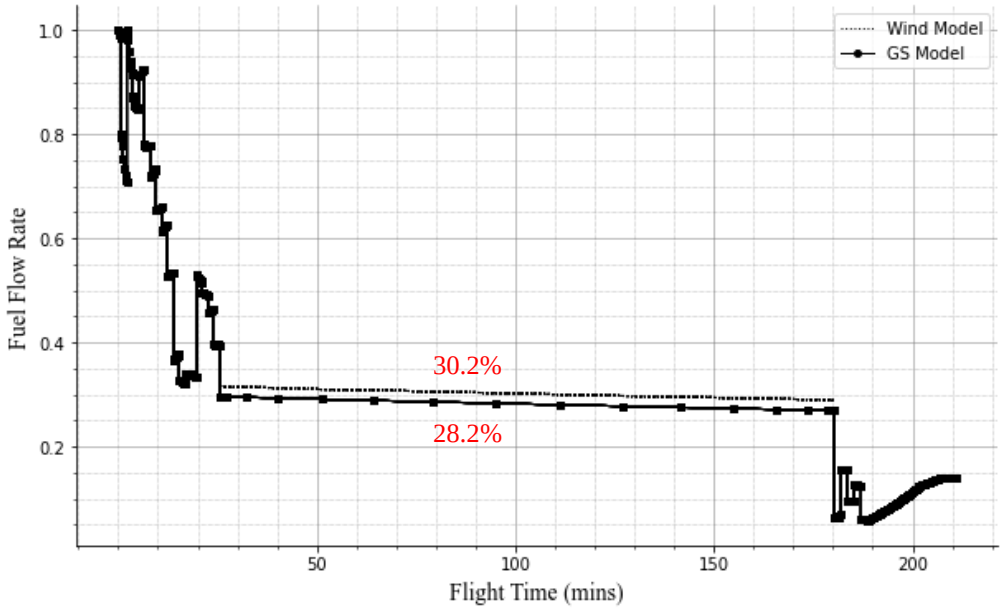

Fig. 7 Comparison of fuel-flow performance for GS model and wind model with a 20 m/s headwind

2. Tailwind

With a 20 m/s tailwind applied, the opposite effect occurred. The TAS became equal to 220 m/s, while the GS was 240 m/s. Using the same logic outlined in the previous paragraph, the GS model used in this study would over-predict the fuel consumption. However, as the drag is dependent on the square of velocity, and wave drag becomes dominant at >0.85 Ma, the over-prediction of fuel consumption for the tailwind mission would be greater than the under-prediction of fuel consumption for the headwind mission This was observed in the results for the tailwind mission presented in Fig. 8, where the GS model produced a normalised fuel-flow rate of 30.7%, while the fuel-flow rate for the wind-modified model reduced to 26.7%. Hence, the fuel-flow error for the GS model for the tailwind flight was 4%, compared to 2% for the headwind analysis. The wind model for the tailwind flight produced a cruise fuel-flow error of 1.6% with respect to the actual flight data, compared to 14% for the GS model.

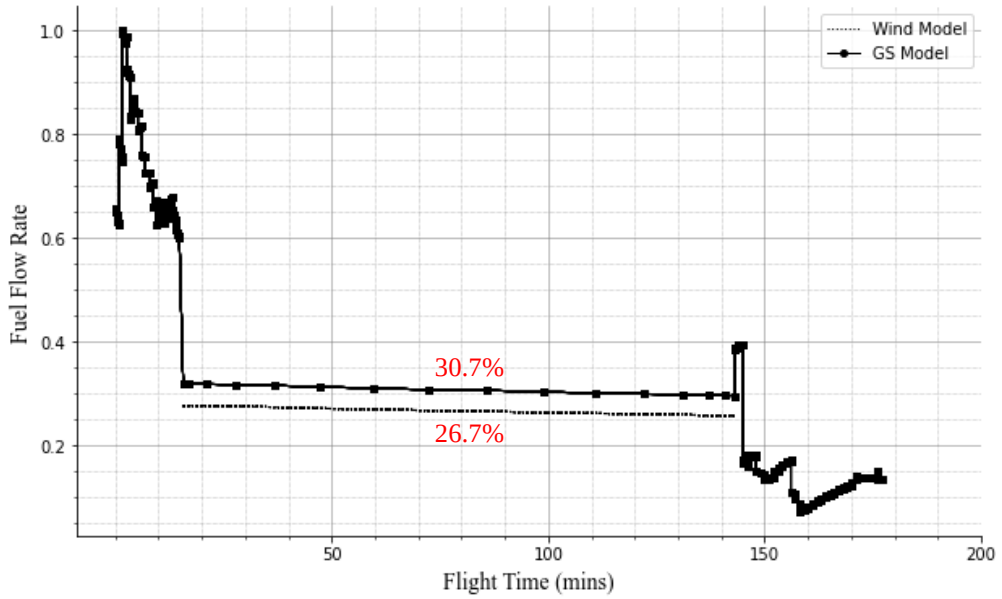

Fig. 8 Comparison of fuel-flow performance for GS model and wind model with a 20 m/s tailwind

The results of this analysis highlights the non-linear characteristics of the fuel burn errors for flights that experience a headwind or tailwind when using the GS model. The non-linear nature of these errors compromised the potential of the SUAVE calibration, as increased drag coefficients yielded a greater effect on the flights that experienced a tailwind, disturbing the error gradients of the optimiser.

V. Calibration

A. Calibration Approach

1. Climb and Cruise

As noted in Section III.B, the 'Fidelity-Zero' aerodynamic method within SUAVE utilised various correction factors to complete the lift and drag calculations. Following the validation of the SUAVE model against real-world flight data, a calibration of these correction factors was performed in order to minimise the fleet-wide fuel burn error. The correction factors include the fuselage and wing parasite drag form factors, along with the fuselage lift, trim drag, and viscous lift-dependent correction factors. The two objective functions were set as the cumulative climb and cruise fuel burn error magnitudes. Setting the objective function as the cumulative fuel burn errors implicitly defined the weighting function of the optimisation problem, as the optimiser prioritised segments and flights with the greatest fuel burn error magnitudes. Furthermore, only the climb and cruise segments were used to calibrate the aerodynamic coefficients, as they represented the most reliable segments of ADS-B data. The multi-objective optimisation problem, including the variable bounds and the optimisation objectives, is described in Table 4. The 'fgoalattain' optimiser within MATLAB was utilised for this analysis. Bounds for the 'Fidelity-Zero' coefficients were kept relatively small to avoid over-fitting and negatively impacting the generalisation capabilities of the calibrated model outside the training cases.

Table 4 Range of calibration variables

Segment	Calibration Vars	Lower	Base	Upper
Climb, Cruise	Fuselage Lift	1.10	1.14	1.16
	Trim Drag	1.01	1.02	1.04
	Wing Drag	1.07	1.10	1.13
	Fuselage Drag	2.25	2.30	2.35
	Viscous Drag	0.36	0.38	0.40
Descent	Minimum Throttle	0.04	0.07	0.08
Initial Climb	T/O $+C_D$	0.00	0.00	0.03
Approach	APP $+C_D$	0.00	0.00	0.03
Final Approach	F-APP $+C_D$	0.00	0.00	0.06

2. Descent

Once the optimum aerodynamic coefficients were obtained, the remaining segments in the descent, initial climb, approach and final approach were calibrated separately via single-objective optimisations. The descent segment was calibrated by setting the minimum idle throttle value to be used when evaluating the fuel-flow from the propulsor surrogate model. The SUAVE code was modified to set the fuel-flow of negative throttle segments equal to the minimum idle fuel-flow, initially prescribed as the fuel-flow for a 7% power operating point at the given altitude and Mach number. It was found that the descent fuel-flow was highly dependent on this minimum idle value, hence the descent segment was calibrated through optimisation of this minimum idle power variable.

3. Initial Climb, Approach, Final Approach

The initial climb, approach and final approach segments required modelling of flaps/slats and landing gear drag, as these were not included in the initial SUAVE model. These segments were calibrated using separate drag increment variables applied to each segment, as outlined in the final three rows of Table 4. These drag increment variables simply

increased the drag coefficient C_D by a prescribed amount. This method of drag modelling is justified as the slats and flap configurations were relatively consistent throughout the flight database.

B. Calibration Results

1. Aerodynamic Coefficients

Table 5 Optimised aerodynamic calibration coefficients

	Fuselage Lift	Trim Drag	Wing Drag	Fuselage Drag	Viscous Drag
Optimum Value	1.10	1.01433	1.07	2.3455	0.40

Table 6 Error reductions for optimised calibration coefficients

Error Value	Base Climb	Opt Climb	Base Cruise	Opt Cruise
Total Fuel Burn	5.4%	4.7%	6.7%	6.1%
Average Fuel Flow	5.4%	4.8%	8.8%	8.2%

The optimised results for the 'Fidelity-Zero' aerodynamic coefficients are presented in Table 5, and the updated fuel-flow and fuel burn errors are presented in Table 6. The base error refers to the cumulative fuel burn error magnitude and average fuel-flow errors for all training cases using the baseline aerodynamic model values presented in Table 4, while the opt error refers to the cumulative fuel burn error and average fuel-flow error magnitude for the optimised calibrated model, using the optimised coefficients outlined in Table 5. Modest fuel burn error reductions of 0.7% and 0.6% were observed for the climb and cruise segments, respectively, which reduced the average fuel-flow error magnitudes for each flight by approximately 0.6%. The optimiser struggled to make a significant impact on the error, as the model was slightly over-predicting cruise fuel burn, while the model was simultaneously under-predicting the climb fuel burn. Hence, the optimiser was working against conflicting objectives which limited the potential solution.

This was likely due to the non-linear error effects as a result of using the GS model. As previously noted, the fuel burn during a tailwind was over-predicted by the GS model, whereas the fuel burn was under-predicted during a headwind, where tailwinds had a greater effect on the fuel burn error. Airlines tend to operate take-off and climb segments with a headwind due to the additional lift obtained, enabling a steeper climb. Conversely, during cruise an airline will aim to maximise the tailwind to save fuel. Therefore, it is possible that these operations, and the lack of TAS available in this model, was the cause of these discrepancies.

2. Minimum Throttle

Table 7 Optimised idle throttle value and error reductions

Calibration Variable	Optimum Value	Base Fuel Error	Opt Fuel Error
Minimum Throttle	0.0592	13.4%	11.0%
		(15.9%)	(12.3%)

The optimised results for the minimum idle throttle value and the associated fuel errors for the descent segment are presented in Table 7. The fuel error value in the first row represents the cumulative fuel burn error, whereas the error value in parenthesis represents the average fuel-flow error of each flight. The baseline model used an idle throttle value of 7%, corresponding with published ICAO test data [37], which was reduced to a value of 5.92% following the optimisation. The cumulative descent fuel burn error was reduced by 2.4%, while the average fuel-flow error magnitude for each flight was reduced from 15.9% to 12.3%.

3. Take-off and Landing Drag

Table 8 Optimised drag increments and error reductions

Calibration Variable	Optimum Value	Base Fuel Error	Opt Fuel Error
T/O $+C_D$	0.0198	11.9%	10.3%
		(12.2%)	(10.4%)
APP $+C_D$	0.0175	12.7%	14.0%
		(11.8%)	(13.8%)
F-APP $+C_D$	0.0569	40.9%	10.5%
		(40.8%)	(10.5%)

The optimised results for the initial climb, approach and final approach drag increment variables and the associated fuel errors are presented in Table 8. The baseline fuel errors correspond to the results with no drag increment to account for deployment of flaps/slats and landing gear. The initial climb segment yielded a modest improvement, with 1.6% of the fuel burn error reduced, improving the average fuel-flow error magnitude from 12.2% to 10.4%. The approach segment error was increased compared to the baseline model due to the change in the minimum idle throttle value, which negatively impacted the approach segment error. The final approach segment yielded significantly improved accuracy with a drag increment of 0.0569, reducing the fuel burn error by >30%. The large drag increment in this phase was required due to high flap deflections and the deployment of landing gear.

C. Calibration Assessment

To assess the performance of the optimised calibrated model, the sum of the total block fuel errors and the average total fuel-flow error of the calibrated model was compared to that of the baseline SUAVE-NPSS model for the 26 training case flights included in the calibration model. Furthermore, three test cases, which were omitted from the calibration training data, were analysed in further detail.

1. Training Data

Table 9 Total fuel burn error reduction for calibrated SUAVE-NPSS model

Model	Total Fuel Burn Error	Average Total Fuel-Flow Error
Baseline	7.5%	5.5%
Optimised	6.3%	4.9%

Table 9 outlines the total fuel burn and average fuel-flow errors for the baseline and optimised model, in which the fuel burn error was reduced by 1.2% through optimisation of the calibration variables outlined in Section V.A. While these error reductions were relatively modest, it must be noted that the lack of TAS in the data limited the potential of the optimisation, as discussed in Section IV.C. Despite this, an average fuel-flow error magnitude <5% with respect to real-world data is considered an acceptable accuracy for conceptual design.

2. Test Cases

Table 10 Total fuel burn error reduction of test cases for calibrated SUAVE-NPSS model

Model	Total Fuel Burn Error	Average Total Fuel-Flow Error
Baseline	6.9%	5.5%
Optimised	6.5%	5.0%

Three test cases of varying range were selected to assess the performance of the calibrated model against unseen data, as highlighted Fig. 1. Table 10 shows that the optimised model generalised reasonably well, with a total fuel burn error reduction of 0.4%. It must be noted that one of these test case flights was the flight analysed in Section

IV.C with strong tailwinds present during cruise. As the optimised calibration tended to increase the fuel consumption of the modelled flights by increasing the drag coefficients, the cruise fuel burn of this test case yielded even greater error following the optimisation. Despite this increase in cruise fuel burn error, the total fuel burn error for the three test flights was still reduced with the optimised model.

The 500 NM test case was analysed in further detail through comparison of validation graphs of the baseline SUAVE-NPSS model and the calibrated SUAVE-NPSS model. Figs. 9 and 10 show validation for the baseline and calibrated model, respectively.

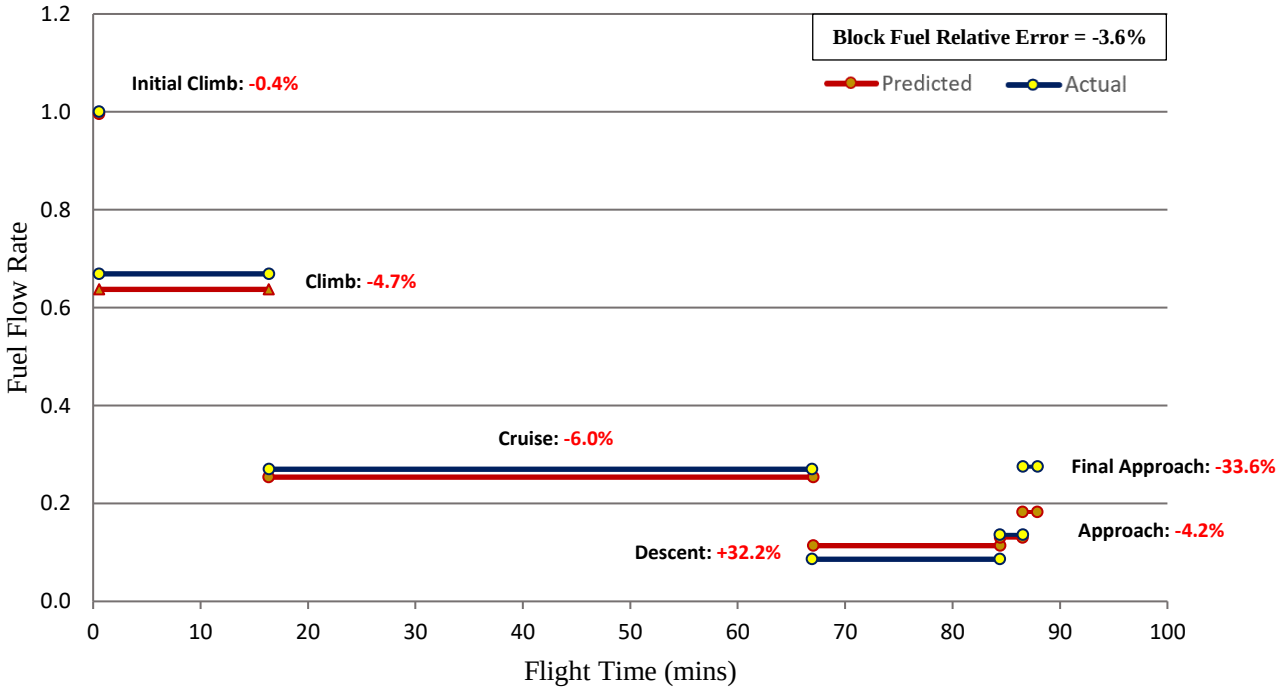

Fig. 9 Validation of baseline SUAVE-NPSS B737-800NG model against actual flight data (500 NM)

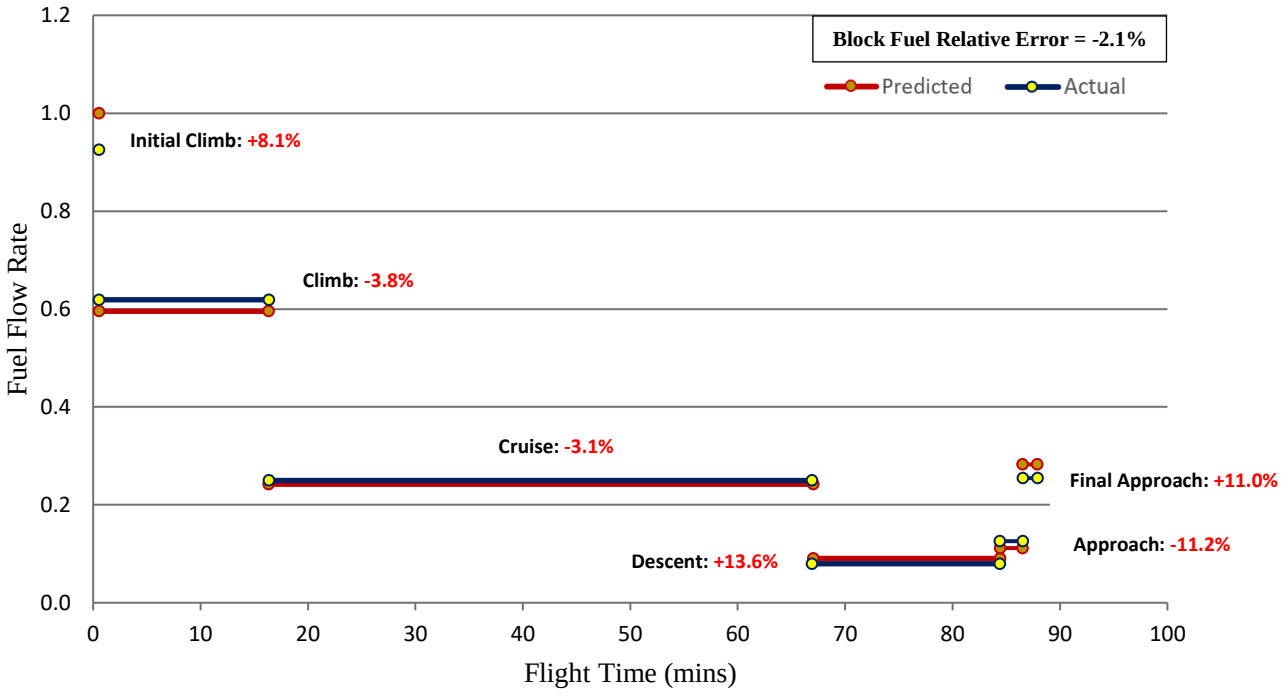

Fig. 10 Validation of calibrated SUAVE-NPSS B737-800NG model against actual flight data (500 NM)

Error reductions were observed for four of the six segments – climb, cruise, descent and final approach, where the greatest error reductions were obtained for the descent and final approach segments, followed by the cruise and climb segments. The error of the initial climb and approach segments was increased, however the length of these segments meant that the fuel consumption error was relatively insignificant. It was clear that the calibration resulting from the optimisation process had an overall positive effect on the model accuracy, which was reflected in the reduced block fuel error – reducing from -3.6% to -2.1%. While the error reductions are highly dependent on the missions selected for validation, and the associated unknown wind speeds for these missions, the results from Table 9 and 10 clearly show that the calibration was successful in enhancing the overall model accuracy for both training and test cases – which was further emphasised in the test-case validations presented in Figs. 9 and 10.

VI. Conclusions

A validation and calibration of the conceptual design tool SUAVE was performed, where the fuel burn accuracy was measured against real-world B737-800NG flight data for 29 flights. The performance of the initial SUAVE model, utilising the standard physics-based 'Fidelity-Zero' VLM aerodynamic model and the built-in propulsion model, was analysed in detail for one flight within the database, and the total error for all flights was obtained. A propulsion model of the CFM56-7B26/3 turbofan was developed and validated against ICAO data, and connected to the SUAVE tool via a surrogate model. The SUAVE-NPSS model was validated against the same flights, where a significant reduction in fuel burn error was observed, indicating the primary source of inaccuracies within the SUAVE propulsion model.

Following the validation, a calibration of the 'Fidelity-Zero' model was performed, in which the aerodynamic correction factors were optimised to minimise the fleet-wide fuel burn error. Further calibration was performed for the minimum idle throttle value of the propulsion model, and the additional drag during the take-off and landing segments to account for the deployment of flaps, slats and landing gear. While the potential of the calibration was found to be limited due to non-linear error effects in the presence of headwinds and tailwinds, the calibration yielded a 1.2% reduction in the fuel burn error magnitude against the training data, resulting in a final error magnitude of 6.3%. The calibrated model was further validated against three test cases of unseen data, in which the total fuel burn error was reduced from 6.9% to 6.5%. The final average fuel-flow error magnitude for the flights modelled was approximately 5%, for both the training and test data. Such a level of accuracy with respect to real-world data is sufficient for conceptual design, hence it can be concluded that SUAVE is a useful tool for modelling unconventional aircraft configurations.

Future work will aim to enhance the calibration through expansion of the flight database to account for a greater number of flights, multiple aircraft configurations, and the inclusion of TAS data. The calibrated model provides an accurate baseline model with respect to real-world flight data, from which future aircraft models with alternative fuel and propulsion systems can be compared. Furthermore, this model provides an accurate and rapid physics-based modelling platform from which advanced propulsion systems and airframe configurations can be assessed and optimised in the context of a full fleet operating over a wide range of scheduled routes, such that confident projections of future carbon reductions can be obtained for new aircraft designs.

Acknowledgments

The authors would like to thank Ryanair for the financial and technical support of this study through the Sustainable Aviation Research Centre at Trinity College Dublin, along with the permission to use their data.

References

[1] "Waypoint 2050." https://aviationbenefits.org/environmental-efficiency/climate-action/waypoint-2050/ (accessed Jul. 05, 2022).

[2] "Sustainable biomass availability in the EU, to 2050," *Concawe*. https://www.concawe.eu/publication/sustainable-biomass-availability-in-the-eu-to-2050/ (accessed Nov. 10, 2022).

[3] E. Cabrera and J. M. Melo de Sousa, "Use of Sustainable Fuels in Aviation—A Review," *Energies*, vol. 15, no. 7, 2022, doi: 10.3390/en15072440.

[4] "Long-term aviation fuel decarbonization: Progress, roadblocks, and policy opportunities," *International Council on Clean Transportation*. https://theicct.org/publication/long-term-aviation-fuel-decarbonization-progress-roadblocks-and-policy-opportunities/ (accessed Sep. 15, 2022).

[5] "FAQS," *Synkero*. https://synkero.com/faqs/ (accessed Nov. 08, 2022).

[6] "Fact Sheet | The Growth in Greenhouse Gas Emissions from Commercial Aviation (2019) | White Papers | EESI." https://www.eesi.org/papers/view/fact-sheet-the-growth-in-greenhouse-gas-emissions-from-commercial-aviation (accessed Apr. 28, 2022).

[7] "Global Electricity Review 2022," *Ember*, Mar. 29, 2022. https://ember-climate.org/insights/research/global-electricity-review-2022/ (accessed Nov. 28, 2022).

[8] "Flight Optimization System (FLOPS) Software v.9(LAR-18934-1) | NASA Software Catalog." https://software.nasa.gov/software/LAR-18934-1 (accessed Nov. 08, 2022).

[9] "TASOPT --- Transport Aircraft System OPTimization." https://web.mit.edu/drela/Public/web/tasopt/ (accessed Oct. 20, 2022).

[10] L. S. Nunez, J. C. Tai, and D. N. Mavris, "The Environmental Design Space: Modeling and Performance Updates," in *AIAA Scitech 2021 Forum*, American Institute of Aeronautics and Astronautics. doi: 10.2514/6.2021-1422.

[11] T. W. Lukaczyk *et al.*, "SUAVE: An Open-Source Environment for Multi-Fidelity Conceptual Vehicle Design," in *16th AIAA/ISSMO Multidisciplinary Analysis and Optimization Conference*, Dallas, TX: American Institute of Aeronautics and Astronautics, Jun. 2015. doi: 10.2514/6.2015-3087.

[12] E. M. Botero, M. A. Clarke, R. M. Erhard, J. T. Smart, J. J. Alonso, and A. Blaufox, "Aerodynamic Verification and Validation of SUAVE," in *AIAA SCITECH 2022 Forum*, in AIAA SciTech Forum. American Institute of Aeronautics and Astronautics, 2021. doi: 10.2514/6.2022-1929.

[13] M. A. Clarke, R. M. Erhard, J. T. Smart, and J. Alonso, "Aerodynamic Optimization of Wing-Mounted Propeller Configurations for Distributed Electric Propulsion Architectures," in *AIAA AVIATION 2021 FORUM*, VIRTUAL EVENT: American Institute of Aeronautics and Astronautics, Aug. 2021. doi: 10.2514/6.2021-2471.

[14] D. Owens, "Weissinger's model of the nonlinear lifting-line method for aircraft design," in *36th AIAA Aerospace Sciences Meeting and Exhibit*, American Institute of Aeronautics and Astronautics. doi: 10.2514/6.1998-597.

[15] S. Karpuk and A. Elham, "Conceptual Design Trade Study for an Energy-Efficient Mid-Range Aircraft with Novel Technologies," in *AIAA Scitech 2021 Forum*, VIRTUAL EVENT: American Institute of Aeronautics and Astronautics, Jan. 2021. doi: 10.2514/6.2021-0013.

[16] Y. Ma, S. Karpuk, and A. Elham, "Conceptual design and comparative study of strut-braced wing and twin-fuselage aircraft configurations with ultra-high aspect ratio wings," in *AIAA AVIATION 2021 FORUM*, VIRTUAL EVENT: American Institute of Aeronautics and Astronautics, Aug. 2021. doi: 10.2514/6.2021-2425.

[17] "Performance analysis of evolutionary hydrogen-powered aircraft," *International Council on Clean Transportation*. https://theicct.org/publication/aviation-global-evo-hydrogen-aircraft-jan22/ (accessed Jun. 08, 2022).

[18] A. Dorsey and A. Uranga, "Design Space Exploration of Blended Wing Bodies," in *AIAA AVIATION 2021 FORUM*, VIRTUAL EVENT: American Institute of Aeronautics and Astronautics, Aug. 2021. doi: 10.2514/6.2021-2422.

[19] A. Dorsey and A. Uranga, "Design Space Exploration of Future Open Rotor Configurations," in *AIAA Propulsion and Energy 2020 Forum*, in AIAA Propulsion and Energy Forum. American Institute of Aeronautics and Astronautics, 2020. doi: 10.2514/6.2020-3680.

[20] "Ryanair | Results Centre." https://investor.ryanair.com/results-centre/ (accessed Sep. 22, 2022).

[21] “Airport Compatibility - Airplane Characteristics for Aiport Planning.” https://www.boeing.com/commercial/airports/plan_manuals.page (accessed Apr. 29, 2023).
[22] “Safran Aircraft Engines,” *Safran*, Apr. 27, 2023. https://www.safran-group.com/companies/safran-aircraft-engines (accessed Apr. 29, 2023).
[23] B. J. Cantwell, “Fundamentals of Compressible Flow”.
[24] R. S. Shevell, *Fundamentals of Flight*. Prentice-Hall, 1983.
[25] R. Shevell, *Introduction to Aircraft Design Synthesis and Analysis*. Department of Aeronautics and Astronautics, Stanford University, 1992.
[26] S. M. Jones, “An Introduction to Thermodynamic Performance Analysis of Aircraft Gas Turbine Engine Cycles Using the Numerical Propulsion System Simulation Code,” NASA/TM-2007-214690, Mar. 2007. Accessed: Oct. 20, 2022. [Online]. Available: https://ntrs.nasa.gov/citations/20070018165
[27] C. E. Rasmussen and C. K. I. Williams, *Gaussian processes for machine learning*. in Adaptive computation and machine learning. Cambridge, Mass: MIT Press, 2006.
[28] A. Dik, N. Bitén, V. Zaccaria, I. Aslanidou, and K. G. Kyprianidis, “Conceptual Design of a 3-Shaft Turbofan Engine with Reduced Fuel Consumption for 2025,” *Energy Procedia*, vol. 142, pp. 1728–1735, Dec. 2017, doi: 10.1016/j.egypro.2017.12.556.
[29] E. Hendricks, “Development of an Open Rotor Cycle Model in NPSS Using a Multi-Design Point Approach,” 2011. doi: 10.1115/GT2011-46694.
[30] G. L. Thomas, D. E. Culley, J. L. Kratz, and K. L. Fisher, “Dynamic Analysis of the hFan, a Parallel Hybrid Electric Turbofan Engine,” in *2018 Joint Propulsion Conference*, Cincinnati, Ohio: American Institute of Aeronautics and Astronautics, Jul. 2018. doi: 10.2514/6.2018-4797.
[31] C. Perullo and D. N. Mavris, “Assessment of Vehicle Performance Using Integrated NPSS Hybrid Electric Propulsion Models,” in *50th AIAA/ASME/SAE/ASEE Joint Propulsion Conference*, in AIAA Propulsion and Energy Forum. American Institute of Aeronautics and Astronautics, 2014. doi: 10.2514/6.2014-3489.
[32] R. P. Thacker and N. Blaesser, “Modeling of a Modern Aircraft Through Calibration Techniques,” in *AIAA Aviation 2019 Forum*, in AIAA AVIATION Forum. American Institute of Aeronautics and Astronautics, 2019. doi: 10.2514/6.2019-2984.
[33] S. Vannoy and C. Cadou, “Development and Validation of an NPSS Model of a Small Turbojet Engine,” Jul. 2016. doi: 10.2514/6.2016-5063.
[34] S. M. Jones, W. J. Haller, and M. T.-H. Tong, “An N+3 Technology Level Reference Propulsion System,” E-19373, May 2017. Accessed: Aug. 09, 2022. [Online]. Available: https://ntrs.nasa.gov/citations/20170005426
[35] “Numerical Propulsion System Simulation (NPSS),” *Southwest Research Institute*, Nov. 07, 2016. https://www.swri.org/consortia/numerical-propulsion-system-simulation-npss (accessed Jun. 08, 2022).
[36] P. G. Batterton, “Energy efficient engine program contributions to aircraft fuel conservation,” presented at the Aviation Fuel Conservation Symp., Washington, DC, Jan. 1984. Accessed: Apr. 29, 2023. [Online]. Available: https://ntrs.nasa.gov/citations/19840021807
[37] “ICAO Aircraft Engine Emissions Databank,” *EASA*. https://www.easa.europa.eu/en/domains/environment/icao-aircraft-engine-emissions-databank (accessed Oct. 20, 2022).